Working title: the most amaz-zing SPIM and how we built it.

M. Caroline Müllenbroich,[a,b] Ludovico Silvestri, [a,c] Leonardo Onofri,[e] Irene Costantini,[a] Marcel Van t'Hoff[f] Leonardo Sacconi,[a,c] Giulio Iannello,[e] Francesco S. Pavone,[a,b,c,d]

[a]European Laboratory for Non-linear Spectroscopy (LENS), University of Florence, Italy
[b]Department of Physics and Astronomy, University of Florence, Italy
[c]National Institute of Optics, National Research Council, Italy
[d]International Center for Computational Neurophotonics (ICON Foundation), Italy
[e]Integrated Research Centre, University Campus Bio-Medico of Rome, Italy
[f]Distrio, Murmex

Abstract. 200 words limit. no numerical references presenting concisely the objectives, methodology used, results obtained, and their significance.

Keywords: Light sheet microscopy, big data, whole brain mounting, data management, whole brain imaging, rolling shutter, 7,8..

Address all correspondence to: First author, University Name, Faculty Group, Department, Street Address, City, Country, Postal Code; Tel: +1 555-555-5555; Fax: +1 555-555-5556; E-mail: myemail@university.edu

1 Introduction

The highly ambitious project of mapping and understanding each and every neuronal connection in the whole brain has been moved from the realm of wishful longing to feasible reality by the recent advent of light sheet fluorescent microscopy (LSFM). With this technique 3D data sets can be acquired with a resolution that is high enough to identify neurons and their dendritic, axonal and spine features in time scales which are no longer the bottle neck of high-throughput acquisition. In LSFM, the sample is illuminated with a thin sheet of light confined into the focal plane of the detection objective, which collects the fluorescence emission along an axis perpendicular to the illumination plane.[1] This technique drastically reduces the imaging acquisition time by recording millions of pixels in parallel and affords optical sectioning by operating fluorescence excitation and detection on separate, perpendicularly oriented paths where the excitation light sheet and the detection focal plane overlap (Figure1,A). Consequently fluorophores outside the light sheet are neither bleached nor contribute blurring out-of-focus noise. Consequently LSFM reduces phototoxicity and photobleaching while achieving excellent resolution at high penetration depths; however, it requires the sample to be transparent.

Several challenges remain to be overcome, however, to allow fast and, most of all systematic, production of reliable datasets and their meaningful interpretation to further our understanding of neuronal networks. Those challenges include fast, cheap and reproducible sample preparation, automated image acquisition that does not require constant attention by an expert and, most crucially, the storage, interpretation and analysis of the unprecedented huge data sets light sheet microscopy routinely produces. The mapping and understanding of this "big data" is a colossal task that requires the expertise of computer scientists to employ fully automated post-processing, for example, to do cell counting or blood vessel segmentation. On the other hand, the imaging of large, intrinsically opaque samples in light sheet microscopy necessitates clearing protocols based

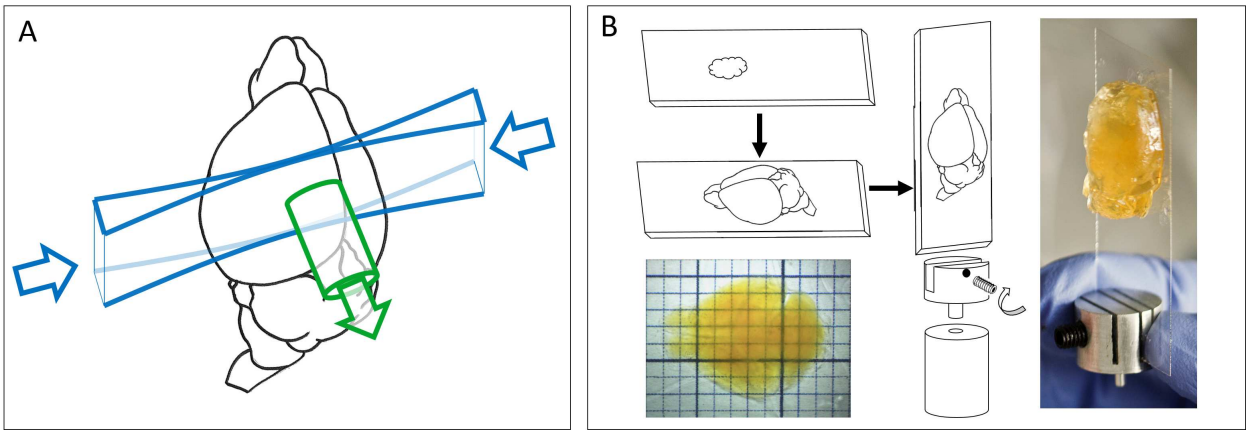

Fig 1: (A) Schematic of light sheet microscopy. Excitation and detection occur on independent perpendicular axes. (B) Mounting of a claried brain. The brain is glued onto a coverslip and inserted into an adapter that slides into a Teflon cylinder.

on refractive index matching which render the tissue transparent. This makes LSFM a truly interdisciplinary field in which the technological advances by optical developers need to be matched by novel development in the area of information and biotechnology.

Here we will describe a state-of-the-art LSFM, as it is implemented in our lab, which can be used to acquire 3D data sets of clarified mouse brains. The LSFM features double-sided illumination with a digitally scanned light sheet and a sample chamber which has been specifically designed for the the imaging of large ($> 1cm^3$), immersed and freely movable samples. After briefly presenting the optical clearing protocol we employ to render our samples transparent, we explain how to prepare and mount the samples for stable, 3D imaging for several days. In addition to a detailed description of all opto-mechanical components, we further present a practical guide for the alignment of a LSFM, a non-trivial task whichhas too often been summarised in a single sentence. A systematic approach to handle, store and analyse the data is also given. We further explain about the data volume we produce how it can be reduced and handled. We finish with some nice data and an outlook. The final sentence of the introduction needs to be amazing.

2 Optical clearing and sample mounting

To elucidate neuronal projections and functional connections in structurally intact tissue it is paramount to be able to image centimeter-sized, clarified samples, such as mouse brains, with high resolution in whole mount preparation. While promising clearing protocols are well documented in literature,[2,3] the question of sample preparation and mounting in light sheet microscopy is not trivial but requires novel approaches to such extent that it is becoming a separate field of research and very diverse strategies such as FEP tubes, 3D printed chambers and Quartz cuvettes have been reported,[3–6] however, these approaches are limited to much smaller sample volumes. The problem of sample mounting in light sheet microscope arises form the fact that optical access to the sample is required from 3-4 planar sides leaving only two opposing sides to insert, fix and move the sample (Figure2,A). Most commonly the vertical direction is chosen. Stable mounting is hereby a key concern as a whole brain tomography can require image acquisition in excess of 24

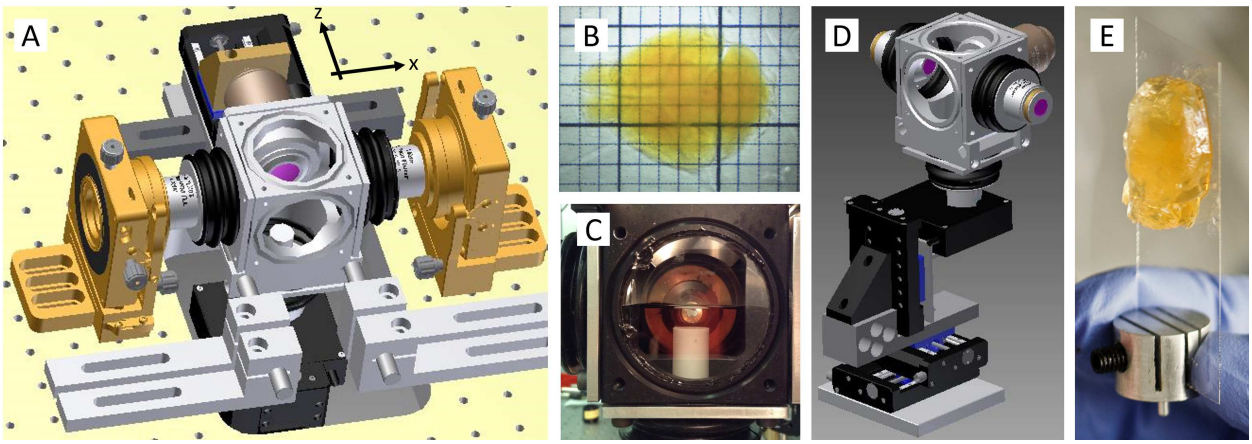

Fig 2: Schematic of light sheet microscopy. (A) Fluorescence excitation (along x axis) and detection (along z axis) are operated on independent, perpendicular light paths where the excitation light sheet and the detection focal plane overlap. The clarified, fluorescently-labelled brain (B) is mounted on a Teflon cylinder inside the watertight chamber (D) and can be translated and rotated freely with piezo motors (D). The sample is glued onto a cover slip which is slid into a custom made adapter mount that is inserted into the Teflon cylinder (E).

hours and the effects of gravity, tissue shrinking/expansion and evaporation of the clearing solution over such time spans might have to be considered.

We designed a cubic, water-tight sample chamber (Figure2,C) that allows access from all six sides while maintaining the 3D integrity of large, clarified and fluorescently-labelled mouse brains. A motorized x-, y-, z-, θ-stage (three M-122.2DD and one M-116.DG, Physik Instrumente) allows free 3D motion and rotation of a Teflon cylinder which reaches into the centre of the chamber (Figure2,D). The clarified brains are fixed with super glue to a coverslip which is slid into a custom made adapter and tightened with a plastic-capped screw. The adaptor is then inserted into the Teflon cylinder (Figure2,E) with the coverslip being positioned on the far side of the detection objective. Three different slits in the adapter correspond to varying distances to the detection objective and give variability in sample thickness for example to allow also for the mounting of rat brain hemispheres. The clarified brains are imaged immersed in clearing solution composed of 63% TDE in Phosphate buffered saline (PBS) and a refractive index of 1.45.

3 Optical path

3.1 Illumination

The custom-made, confocal light sheet microscope is equipped with 5 linearly polarised, cw lasers for fluorescence excitation (Figure3,A). The wavelengths were chosen to excite the most common fluorophores (see Table1 for the manufacturer and specifications of opto-mechanical components). The laser light from each laser is first collimated and expanded with a telescope (f140, f200) and then combined into a common path with a beam steering mirror and a long-pass filter (Semrock, LaserMUX^{TM} series). An acousto-optical tunable filter (AOTF) acts as fast (μs) electronically tunable filter which uses the acousto-optical interaction inside an anisotropic medium to select and transmit any combination of up to four of the laser lines. The radio-frequency applied on the AOTF

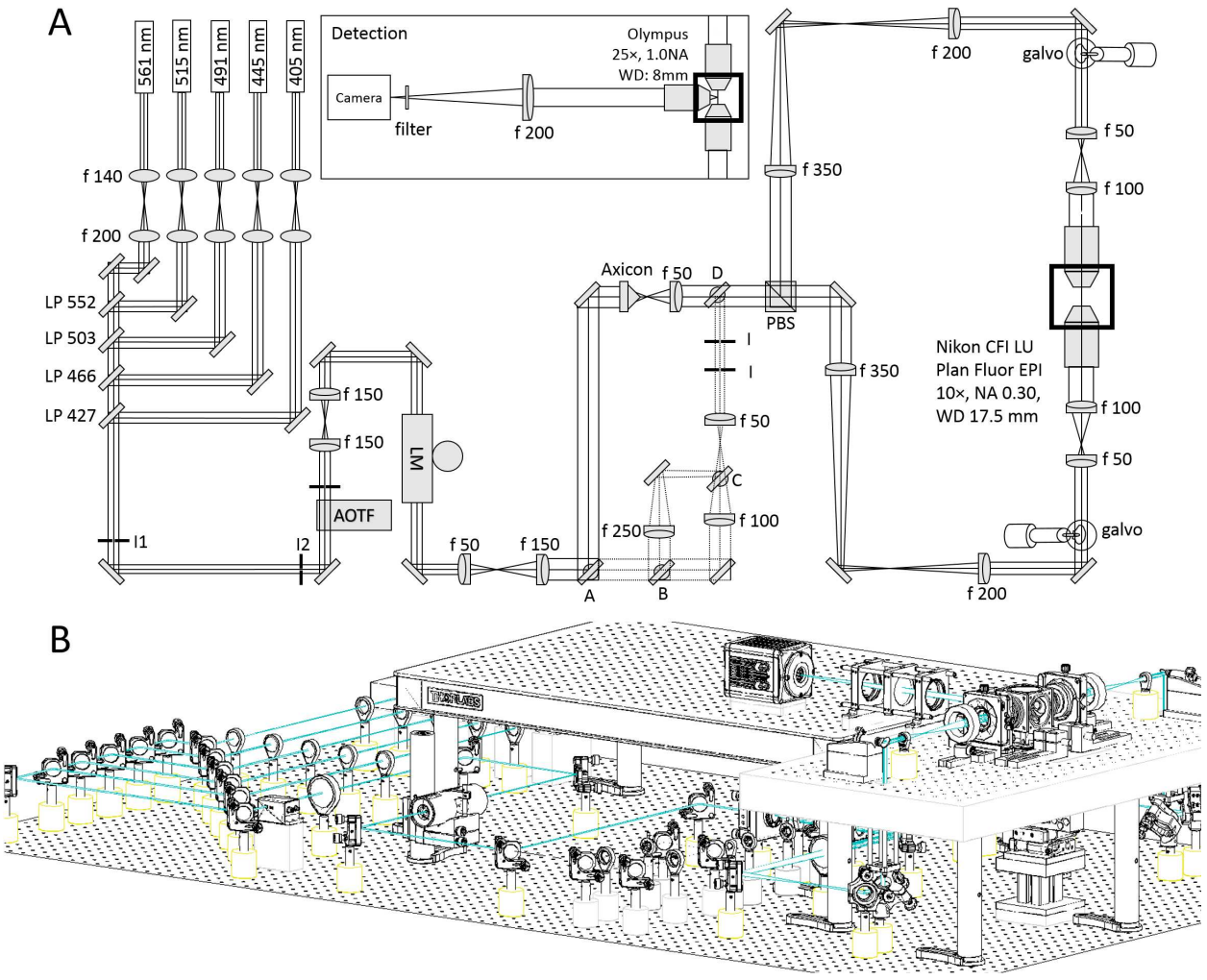

Fig 3: (A) Topview of the excitation path. The galvo scanners are mounted above periscopes. LP: long-pass filter, I: iris, AOTF: acousto-optical tunable filter, LM: laser modulator, PBS: polarisation beam splitter, ABCD: flip mirrors. Inset: detection. (B) Oblique view of the microscope. A custom-made breadboard serves to mount the sample chamber and objectives at an elevated height and features two circular holes at the edges for the periscopes and a large central cut out for the translation stages. A second breadboard is used for the camera.

transducer controls the wavelength being transmitted into the first order and the radio-frequency amplitude allows to adjust the transmitted light intensity. Due to the nonlinear response of the AOTF we measured the AOTF light transmittance for each wavelength as a function of radio frequency amplitude and determined a look-up table to linearise the output. The zero order light is blocked by an iris. An electro-optical laser modulator acts like a wave plate with electrically controlled retardation and rapidly rotates (few hundreds ns) the input polarisation of the excitation light by $90°$. The wavelength-dependent, high voltage that needs to be applied to the birefringent crystal inside the modulator to change the optical path length is provided by a two-step pre-amplification system. First, a low voltage, analog signal from the DAQ board is pre-amplified with custom made electronics and then fed into a commercial high voltage amplifier. A digital line is used to electronically control the frequency of the polarisation shift. After the laser modulator the excitation beam is further expanded by a factor of 2 (f100, f200) with two achromatic doublets.

From here on three different light paths can be chosen through flip mirrors. One light path option guides the light through an axicon (apex angle of $160°$) and an achromatic doublet (f50) to create a Bessel beam. The other two options create Gaussian beams of different beam diameter. This diameter variation translates to different fields of view later on in the detection path. The three options are recombined before a polarising beam splitter cube which splits the excitation light depending on its polarisation into one of the two excitation arms which are built to be identical. The beam is reduced with a telescope (f350, f200) whose telecentric plane coincides with the mirrored surface of a galvanometric scanner (galvo). The galvos are mounted on a custom made optical breadboard which features two circular holes to pass the periscopic beams and a large central cutout for the sample chamber and motor stages. The light sheet is generated digitally by scanning the excitation beam with a sawtooth signal applied to the galvo. This generates perfectly incoherent illumination resulting in fewer artefacts.

The scan mirror surface is reimaged with a telescope (f50, f100) onto the back aperture a long working distance, low magnification objective (Nikon, 10x 0.3NA WD 17.5mm). The two excitation objectives are designed for air immersion. A coverslip glued to the front housing edge serves the dual purpose of maintaining the first diffractive surface between the front optical element and the air and to protect the front lens elements from the organic solvent. The sample chamber is tightly bolted to the optical breadboard while soft connections through silicone bellows allow for adjustive movements of the objectives and free 3D motion of the motor stages. All connections are sealed with rubber rings and silicone caulk and additionally tightened with cable binders. In this way the objectives can be refocused and realigned without compromising the watertight seal of the chamber.

3.2 Detection

Fluorescence is collected on a axis perpendicular to the excitation with an objective that was specifically designed for immersion in clearing solutions of various refractive indices. The objective is equipped with a correction collar allowing for immersion in media with refractive indices ranging from 1.41 to 1.52 (Olympus, XLSLPLN25XGMP). To image the whole volume of interest the objective has a relatively low magnification of 25x and a large working distance of 8mm yet a high numerical aperture (1.0NA) affords high resolution imaging. HERE WE'LL NEED SOME CHARACTERISATION DATA. An overview of imaging properties and derived quantities is given in Table2. We use a tube lens of 200mm to create an image on a sCMOS camera (Orca Flash4.0,

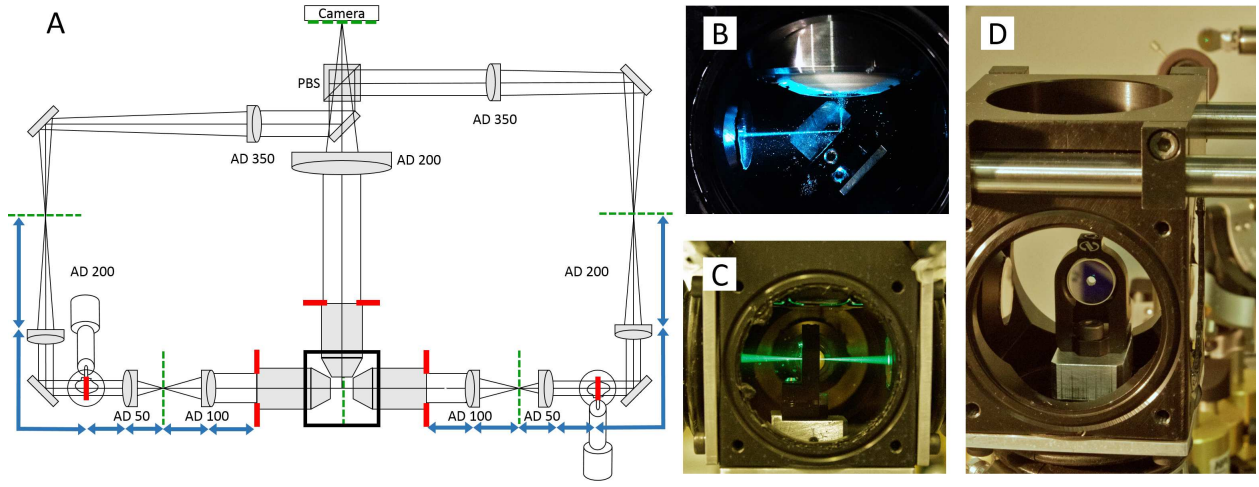

Fig 4: (A) Basic geometrical optics of a double-sided illumination light sheet microscope. AD: achromatic doublet, PBS: polarising beam splitter, red: objective back focal planes and conjugated telecentric planes, green: image planes, blue: 4f telecentric lens system. (B) The alignment mirror can be rotated to precisely reflect at $45°$. (C) With lateral movement the alignment mirror can be placed such that light is transmitted into the opposing excitation arm. (D) Alignment mirror with drilled hole for light transmission, mount for tip adjustment and adaptor for the Teflon tube.

Hamamatsu). A fluorescent filter is used to block out any excitation light. The camera chip of over 4 megapixels is read out in one sweep from top to bottom in the so-called light sheet mode in which only a subset of horizontal lines is exposed and consequently read out and any time. This sweeping line exposure creates a virtual confocal slit. Confocality is achieved by synchronising a single line which generates the light sheet with the exposure of a few lines on the CMOS chip.

3.3 Alignment

For light sheet microscopy it is crucial that excitation and detection occur on perpendicular axes because any deviation from this geometry results in obscured images of reduced resolution and contrast. The objectives need to be perfectly confocal so that the fluorescence that is generated in the swept excitation beam also falls within the detection objective's depth of field. Telecentricity, that is the imaging with two lenses which are the sum of their focal lengths apart, has to be strictly observed in all three arms (Figure4,A), which means the galvo scanners need to be precisely placed in telecentric planes of the excitation objectives while in the detection path, the camera chip needs to be positioned in an image plane of the detection objective. Additionally, homogeneous illumination from both sides impose strict symmetry considerations on both illumination arms that have not only to be sufficiently aligned within themselves respectively but function as pair with recursive dependence.

Our microscope was aligned with two tools, a shear plate to qualitatively assess collimation and a small mirror that can be mounted inside the sample chamber where the sample would usually be. The 0.5in mirror was first pierced with a drill using a ceramic drill bit to produce a hole roughly in its centre of the approximately the same diameter as the excitation beam inside the sample chamber. Using a compact single axis adjustable mirror mount (V50-AX, Newport) attached

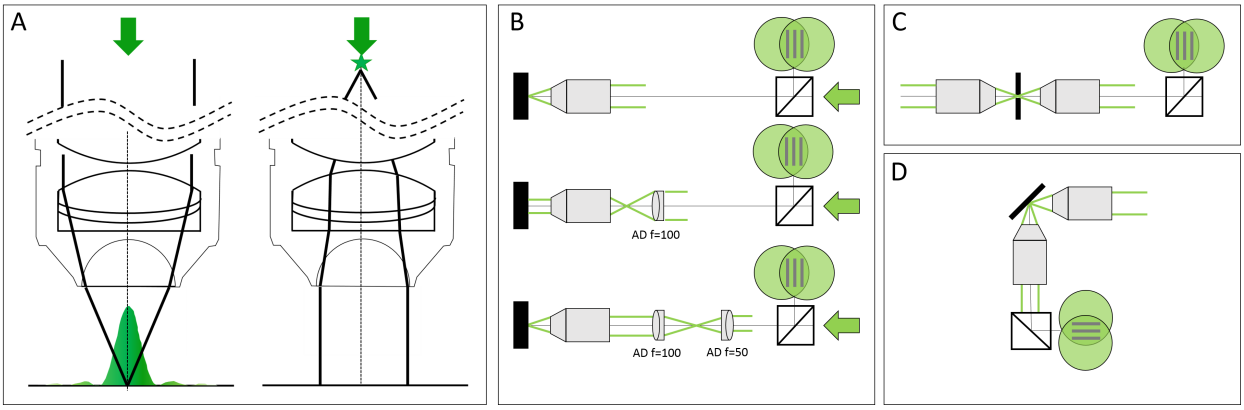

Fig 5: (A) Working principle of a microscope objective (left): a collimated input beam in converted into a spherical wavefront. Right: inverted light path where a focal spot in the back aperture creates a collimated output. (B) Recursive placement of lenses using the sample mirror in back-reflection mode, (C) in transmission mode and (D) in reflection mode.

to the Teflon cylinder inside the chamber allows to to adjust the pitch of the reflection with the mount and the yaw with the rotation stage while at the same time providing a very space efficient mounting for the pierced 0.5in mirror. With this "sample mirror" three different position can now be easily implemented, firstly, back reflection by hitting the reflective surface at $0°$, secondly, transmission by laterally displacing the mirror until the light passes through the drilled hole, and thirdly, reflection of the light by $90°$ by precisely turning the mirror mount by $45°$ using the rotation stage.

The excitation objectives are fixed on mounts which allow three dimensional translation plus pitch and yaw adjustment (LP-1A, Newport). In a first step the beam paths of both excitation arms where brought to overlap through irises placed on the breadboard and the optical bench without any microscope objectives. We found it useful to use two mirrors in each periscope, one vertically mounted and one mounted at $45°$ for vertical deflection of the incoming beam. In this way full beam steering can be achieved to realign the periscope before hitting the galvo scanner. After this initial alignment the first excitation objective was then placed into the beam path and brought to focus onto the sample mirror, which was adjusted to reflect the light back into the same objective. Using a shear plate and a beam splitter cube the back reflected light was qualitatively checked for collimation to ensure the sample mirror was correctly placed in the focal plane of the objective (Figure5,B). The sample mirror was then moved laterally to allow the excitation beam to pass through the drilled hole and the second excitation objective was placed (Figure5,C). This time collimation was checked with the light going through both objectives and so their confocal placement was insured. The microscope was then aligned recursively by starting at the putative confocal point between the objectives and placing successively lens after lens in the direction towards the light source. Finally, the sample mirror was position in reflection mode and the detection objective was aligned (Figure5,D).

4 Optical characterisation

5 Data

Everybody take a look at Figure6 because it is the best we have.

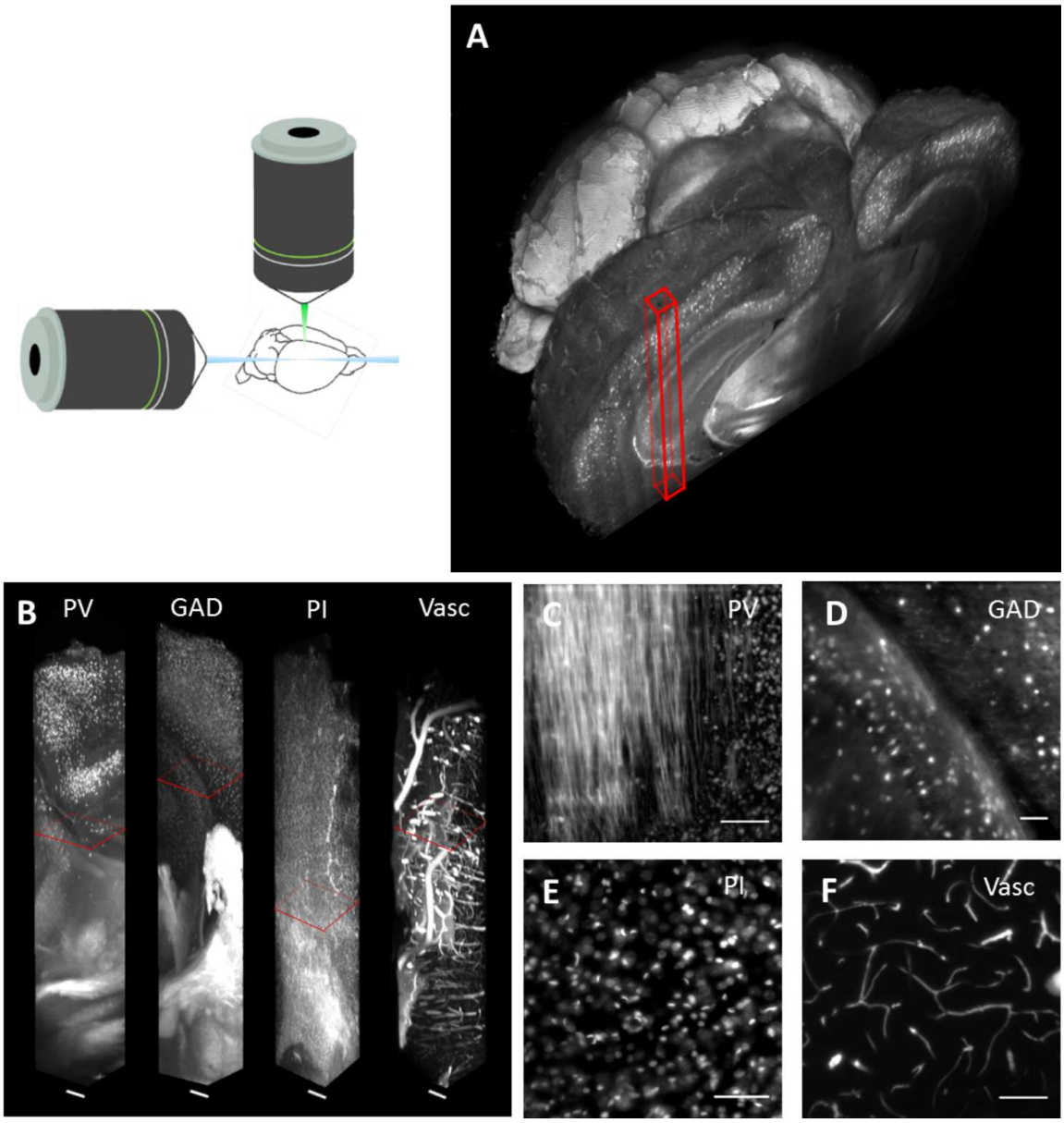

Fig 6: Whole mouse brain tomography. Imaging of whole transgenic mouse brains treated with CLARITY and cleared with TDE 63% imaged with LSM (Olympus, 25X objective). (A) 3D rendering of a parvalbumin-dTomato brain. (B) 3D rendering of stacks from PV-dTomato mouse brain, GAD-dTomato mouse brain, PI stained mouse brain, FITC-albumin labeled mouse brain, scale bar = 400 m. (C,D,E,F) High resolution insert, of the stack corresponding to red boxes in C. Scale bar = 100 m.

6 Conclusion

summary Light sheet microscopy has already been a game changer for large-scale imaging by yielding data with a combination of unprecedented spatio-temporal scale. The impact of this unique measurement technique will continue to revolutionise the field of whole brain connectomics due to its ability to record millions of images over the course of days or even weeks. The data produced in this fashion easily amounts several TB per data set and needs to be stored, transferred, retrieved, processed and visualised necessitating the concurrent development of novel computational interface and analysis methods. The latter need to be robust, standarised and fully automated processes yet allow for flexible, exploratory and tailored analysis.

7 Outlook

where are we going next with this? ask Leo Onofri and Giulio to contribute to this, issues data mangament, aberration correction mapping of complementary data sets obtained in the same system, eg structural connectivity, morphology and gene expression.

Table 1: Overview of optomechanical components.

Component	Manufacturer	Part#	Specifications
Lasers	Cobolt AB, Sweden	MLD	405nm (for DAPI), 80mW, s-polarised
		MLD	445nm (for CFP), 50mW, s-polarised
		Calypso	491nm (for GFP, FITC), 50mW, s-polarised
		Fandango	515nm (for Venus, YFP), 50mW, s-polarised
		Jive	561nm (for dTomato, PI, RFP), 50mW, s-polarised
AOFT	AA Opto-Electronic, France	AOTFnC-400.650-TN	$> 90\%$ diffraction efficiency, 3nm resolution, low cross talk between laser lines, high separation angle
Laser modulator	Qioptiq GmbH, Germany	LM 0202 VIS ADP	400-650nm , $\lambda/2$-voltage (633nm): 210V
Pulse amplifier	Falco Systems, The Netherlands	WMA-300	50x amplification up to $\pm$ 150V, DC to 5MHz signal bandwidth
Galvo scanner	Cambridge Technology, USA	6220H	small angle step response $200\mu s$
Objectives	Nikon; Japan	Plan Fluor EPI	10x0.3NA, WD 17.5mm, EFL 20mm (excitation)
	Olympus, Japan	LMPLFLN20X	20x0.4NA, WD 12mm, EFL 9mm (detection)
Motor stages	Physik Instrumente, Germany	C-863.11	DC servo-motor controller
		M-122	Travel range 25mm, $0.1\mu m$ resolution, max. velocity 20mm/s
		M-116	Precision Rotation Stage, $2.5\mu rad$, max. velocity $20°/s$
Camera	Hamamatsu, Japan	Orca Flash4.0	sCMOS sensor, 2048(H) x 2048(V), cell dim.: $6.5\mu m$, active area: 13.3mm x 13.3mm, 16bit images
DAQ board	National Instruments, USA	NI PCIe-6353	AI: 1 MS/s multichannel; 16-bit resolution, 10 V; AO: 2.86 MS/s, 16-bit resolution, 10 V; digital I/O lines (hardware-timed up to 10 MHz), 100MHz max counter frequency
Workstation	Dell, USA	T7500	12GB RAM, Intel Xeon Processor X5647 @ 2.93 GHz, 64bit OS, Win7

Table 2: Imaging properties and derived quantities. The thickness of the light sheet is approximately of the same size as the depth of field of the high NA detection lens.

Detection				
wavelength	λ		0.5	μm
refractive index	n		1.45	
numerical aperture	NA_d		1	
angular aperture	α	$= sin^{-1}(\text{NA}_d/n)$	43.6	deg
magnification	M		25	
tube lens	f_{TL}		180	mm
effective focal length objective	EFL	$= f_{\text{TL}}/M$	7.2	mm
diameter back focal plane	BFP	$= 2\text{EFLNA}_d$	14.4	mm
field number	FN		18	mm
field size in specimen	S	$= \text{FN}/M$	0.72	mm
depth of field	Δ	$= \lambda * n/(\text{NA}_d)^2 + n * e/M\text{NA}_d$	1.10	μm
Airy radius lat.	r_A	$= 0.61\lambda/\text{NA}_d$	0.31	μm

Excitation				
numerical aperture	NA_e		0.3	
magnification, nominal	m		10	
tube lens	f_{tl}		100	mm
effective focal length, objective	efl	$= f_{\text{tl}}/m$	20	mm
magnification, effective	m_e	$= f_{\text{tl}}/\text{efl}$	5	
refractive index	η		1	
beam radius	ω		4.5	mm
min light sheet waist	ω_0	$= \lambda\text{efl}/\pi\omega$	1.41	μm
confocal parameter	b	$= 2\pi\omega_0^2/\lambda$	25.15	μm

Camera				
cell size	e		6.5	μm
effective area	r^2		13.3^2	mm^2

Acknowledgments

Human Brain Project tutta la vita. GARR gave us a beautiful 10gb fiber to cineca CINECA for hosting us on pico

References

1 J. Huisken and D. Y. Stainier, "Selective plane illumination microscopy techniques in developmental biology," *Development* **136**(12), 19631975 (2009). 1

2 K. Chung, J. Wallace, S. Y. Kim, S. Kalyanasundaram, A. S. Andalman, T. J. Davidson and K. Deisseroth, "Structural and molecular interrogation of intact biological systems," *Nature* **497**(7449), 33233 (2013). 2

3 R. Tomer, L. Ye, B. Hsueh and K. Deisseroth, "Advanced CLARITY for rapid and high-resolution imaging of intact tissues," *nature protocols* **9**(7), 1682-1697 (2014). 2

4 A. Kaufmann, M. Mickoleit, M. Weber and J. Huisken, "Multilayer mounting enables long-term imaging of zebrafish development in a light sheet microscope," *Development* **139**(17), 3242-3247 (2012). 2

5 P. Pitrone, J. Schindelin, L. Stuyvenberg, S. Preibisch, M. Weber, K. W. Eliceiri, J. Huisken and P. Tomancak, "OpenSPIM-an open access platform for light sheet microscopy," *arXiv* reprint arXiv:1302.1987, 3242-3247 (2013). 2

6 O. E. Olarte, J. Licea-Rodriguez, J. A. Palero, E. J. Gualda, D. Artigas, J. Mayer and P. Loza-Alvarez, "Image formation by linear and nonlinear digital scanned light-sheet fluorescence microscopy with Gaussian and Bessel beam profiles," *Biomedical optics express* **3**(7), 1492-1505 (2012). 2

7 L. Silvestri, A. Bria, L. Sacconi, G. Iannello, and F. S. Pavone, "Confocal light sheet microscopy: micron-scale neuroanatomy of the entire mouse brain," *Opt Express* **20**(18), 20582-20598 (2012).

8 P. Frasconi, L. Silvestri, P. Soda, R. L. Cortini, F. S. Pavone and G. Iannello, "" *Bioinformatics* **30**(), i587-i593 (2014).

9 A. Bria and G. Iannello, "TeraStitcher-A tool for fast automatic 3D-stitching of teravoxel-sized microscopy images," *BMC bioinformatics* **13**(1), 316 (2012).

List of Figures

List of Tables